NbN Superconducting Single Photon Detectors

John Y. Shin*
University of California, Santa Cruz†
(Dated: August 31, 2015)

The NV^- center in diamond is a well-studied qubit system with applications in quantum information processing and magnetometry. Among the current fronts of research in quantum information processing is the entanglement of these NV^- center defects. To this end, on-chip single photon detectors are a necessary step towards quantum gates and scalability. Our system incorporates gallium phosphide waveguides to route the photon emissions from the NV^- centers. We intend to implement waveguide-coupled niobium nitride superconducting single photon detectors for on-chip detection. Theoretical and experimental results are examined to narrow the region of interest, and FDTD simulations are used to calculate the absorption probability.

INTRODUCTION

The NV center is a defect in diamond where a nitrogen replaces a carbon atom and there is an adjacent vacancy at a lattice site [4]. Initially charge neutral, a captured electron makes the charge state negative. The defect has many attractive properties as a qubit, including long-lived spin quantum states and well-defined optical transitions [2]. Our system incorporates gallium phosphide waveguides and disk resonators [24] as a photonic network over the diamond substrate, as seen in Figure 1.

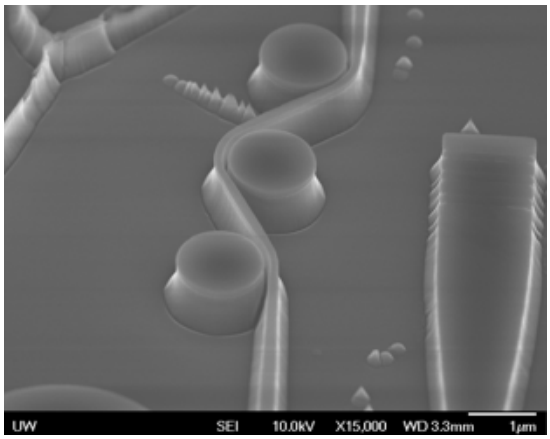

Figure 1: GaP disc resonators and waveguides, lab sample.

Our goal is to implement waveguide-coupled niobium nitride superconducting single photon detectors (SSPDs) as a step towards many-qubit entanglement and scalability. SSPDs are quasi-2D nanowires with thicknesses on the order of nanometers, widths near 100 nm, and lengths on the order of microns. We simulate the absorption probability as a function of the geometry of these detectors.

SSPDS AND SIMULATIONS OF THEIR DEVICE EFFICIENCY

Superconducting single photon detectors (SSPDs) allow on-chip detection of individual photons, a key component of quantum information processing. Our system will implement SSPDs in the "traveling wave" design, where the nanowire is placed in a single U shape on top of a GaP waveguide, which lies on top of a diamond substrate, as in Figure 2.

Figure 2: Detector design. The blue object is the detector, the red layer is the waveguide, and the gray layer is diamond.

To this end, a detector with high device detection efficiency (DDE) is necessary (the fraction of photons already propagating in the waveguide which can be registered). The DDE can be separated into two components [6]:

$$\eta_{dde} = \eta_{abs} \times \eta_{reg} \tag{1}$$

Where the first term is the probability that a photon will be absorbed, and the second term is the probability that this event will register a count. The first quantity can be naively made to approach unity by increasing the length, width, and thickness of the detector [15]. The second quantity can be naively optimized by decreasing the width and thickness of the detector [15]. We note that some papers also incorporate the probability that

the photons couple into their waveguide into their device efficiency [6], and the nomenclature for both these terms can vary.

Niobium nitride (NbN) nanowires have been implemented as SSPDs in silicon and other systems. A "traveling wave" detector design allows maximization of the probability of absorption.

The photon detection mechanism in NbN nanowires is currently debated in the literature. The general mechanism is that the absorption of the photon causes either suppression or breaking of the superconductivity, and, aided by vortices, this causes the biased detector to experience a voltage spike. Though the finer details of the detector physics involves microscopic quantum mechanics, the absorption characteristics (η_{abs}) of the detector can be simulated and optimized with finite difference time domain (FDTD) simulations of Maxwell's equations. These simulations, guided by the theoretical models, provide a guideline for the fabrication process. The difficulty of simulating the detector lies in the fact that the detection mechanism is still debated [18, 21], and while FDTD simulations can be used to optimize the absorption of the detector, η_{reg} cannot be easily simulated.

There are two proposed models of the detection mechanism with two varieties of each: the hotspot model with and without magnetic vortices, where the superconductivity is completely suppressed in a cylindrical region, and the diffusion model with and without magnetic vortices, where the superconductivity is suppressed over a wider region that crosses the width of the detector [18]. In the first model, the minimum threshold for the bias current necessary for a constant detection probability is related to the photon energy by [6]:

$$(1 - I_{th}/I_c) \propto \sqrt{E} \tag{2}$$

While in the second model it is related by:

$$(1 - I_{th}/I_c) \propto E \tag{3}$$

Thus, the relationship between photon energy and relative current can be used for model analysis. Even with the assumption of one of the models, many of the parameters of the models require very coarse assumptions, i.e., the relationship between the photon energy and the size of the suppression/breaking of the superconductivity, the distribution of the quasiparticles, and the amount of quasiparticles created during the event.

To truly simulate η_{dde}, η_{reg} would need to be simulated along with η_{abs}. We examine theoretical models and experimental data to refine our optimization of η_{abs}, but do not calculate η_{reg} directly.

SUPERCONDUCTIVITY OF NBN AND GEOMETRIC CONSTRAINTS

Superconductors are known for their zero resistance under a critical temperature, T_c, which is defined to be the middle of the transition towards zero resistance. In Figure 3, we see the normalized resistance as a function of temperature for a 6 nm thick lab sample.

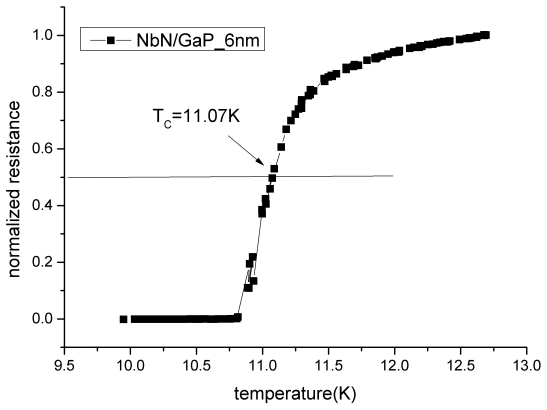

Figure 3: NbN on GaP Critical Temperature, Lab Sample

NbN superconductivity can be described by the type-II BCS theory [25] and Ginzburg-Landau theory. The Ginzburg-Landau theory is a model of macroscopic superconductivity which falls out of BCS theory near T_c and when spatial variations of the superconductivity are not too rapid. As a quasi-2D system, novel phenomena also emerge (namely the KT transition [22]).

We first define Pippard's coherence length, which can be derived from a few simple arguments. Since electrons participating in the superconductivity must be approximately within kT_c of the Fermi surface, their momentum range is approximately $\delta p \approx kT_c/v_F$, where v_F is the Fermi velocity. Using the uncertainty relation, we find:

$$\delta x = \xi_0 = a\frac{\hbar v_F}{kT_c} \tag{4}$$

Where a is predicted to be 0.18 by BCS theory. Roughly speaking, this denotes Cooper pair size. A "dirty" superconductor is when the electron mean free path l is much less than Pippard's coherence length, ξ_0. This limits the effective coherence length of the cooper pairs, and leads to an increased penetration depth for fields.

There is a second coherence length, called the Ginzburg-Landau coherence length, which characterizes the distance over which the superconducting wavefunction can vary. We shall call this $\xi(T)$. This quantity

approaches ξ_0 at $T \ll T_c$. Using the London equations, we find that magnetic fields are exponentially screened from the interior of a superconductor with penetration depth $\lambda_L(T)$. The ratio of these two parameters $\kappa = \frac{\lambda}{\xi}$ is called the Ginzburg-Landau (GL) parameter.

Type II superconductivity is where the GL parameter satisfies $\kappa = \frac{\lambda_L}{\xi} > \frac{1}{\sqrt{2}}$, which corresponds to the transition to negative surface energy.

The Ginzburg-Landau theory introduces a complex order parameter $\psi = |\psi|e^{i\theta}$ where $|\psi|^2$ is equal to the local density of superconducting electrons [23]. The GL equations are:

$$\begin{aligned} \alpha\psi + \beta|\psi|^2\psi + \frac{1}{2m^*}\left(\frac{\hbar}{i}\nabla - \frac{q^*}{c}\vec{A}\right)^2\psi = 0 \\ \vec{J_s} = \frac{q^*}{m^*}|\psi|^2\left(\hbar\nabla\phi - \frac{q^*}{c}\vec{A}\right) = q^*|\psi|^2\vec{v_s} \end{aligned} \tag{5}$$

We can see that $\vec{J_s}$ appears to be equivalent to the one-particle equation with an effective mass and charge, where the starred terms are merely double the values for the electron. The first equation reduces to the Schroedinger equation with eigenvalue $-\alpha$ when the nonlinear term is removed. The nonlinear term acts like a repulsive potential of ψ on itself, spreading it out uniformly, which is an intuitive result of Coulomb repulsion. When removing the third term in the first equation, we also find that $|\psi|^2 = \frac{-\alpha}{\beta}$. The physical meaning of this ratio can be understood as the wave-function value infinitely deep in the interior of the superconductor, where it is screened from any surface currents or fields. Future work could be done to couple these equations to the absorption rates [21, 26], or to couple the absorption rates to a quasiparticle diffusion model [6].

The quantity, α, is also related to the GL coherence length by:

$$\xi(T) = \sqrt{\frac{\hbar^2}{2m^*|\alpha(T)|}} \tag{6}$$

For the interest of geometric constraints, we are primarily interested in the GL coherence length. Of interest are also the superconducting bandgap, $\Delta(T)$, and the critical/depairing current, I_c. To suppress or break the superconductivity, the energy of the photon must satisfy:

$$E = \frac{hc}{\lambda} \gg \Delta \tag{7}$$

Since our photon energy is on the order of eV and the superconducting bandgap on the order of meV, this is readily satisfied. A naive upper-bound on the number of quasiparticles, N_{qp}, created by the event is E/Δ. In reality, there is a conversion factor depending on the wavelength of the photon $N_{qp} = \frac{\zeta hf}{\Delta}$, where ζ is on the order of 0.15 [5]. For the detection mechanism, the detector must be biased to near I_c, and a subsequent absorption of a photon exceeds the threshold, creating a voltage spike across the detector. An estimate of the critical current, in the approximation $\xi \ll w$ can be given by [3]:

$$I_c = \frac{\phi_0 w}{e\pi\mu_0\xi\Lambda} \tag{8}$$

Where Λ is the Pearl length ($2\lambda_L^2/d$, where d is the thickness), w is the width of the detector, ϕ_0 is the magnetic flux quantum, e is the base of the natural logarithm, and ξ is the GL coherence length. The Pearl length is a length scale for Pearl vortices, and since $w \ll \Lambda$, we can ignore current-induced magnetic fields [7].

Next, we shall impose constraints on the geometry of the detector to narrow the region of interest for our simulations.

The thickness of the detector is a complex interplay between T_c, I_c, η_{abs}, and η_{reg}. A thicker detector improves T_c, I_c, and η_{abs}, while a narrower detector improves η_{reg}. In an email, J.J. Renema suggests that we do not stray from 4-5 nm. We can also consider the fact that we want to keep any suppression/breaking of the superconductivity uniform over the thickness of the wire. As such, we would want to keep the thickness close to the Ginzburg Landau coherence length, $\approx 5\,nm$ [6].

Next, we examine width constraints. The existence of magnetic vortices in the detector is predicated on the width of the detector satisfying the relationship: [22]

$$w > 4.4\xi_{GL}(T) \tag{9}$$

Where $\xi(T)$ is the Ginzburg-Landau coherence length taken at ambient temperature. Since these vortices are thought to play an important role in the detection mechanism [18], we can use this as a coarse lower bound on our detector widths.

Next, we must assume a model to allow us to constrain the width of the detector with an upper bound. We assume the hotspot model. Under this model, we find that the diameter of the hotspot must be large enough such that the current around it breaks the critical current density. This can be stated:

$$D > w\left(1 - \frac{I_b}{I_c}\right) \tag{10}$$

Where I_b is the current bias, I_c is the critical current, w is the width of the nanowire, and D is the diameter of the hotspot. If we assume a two-dimensional hotspot, the surface area of our hotspot is proportional to the energy of our photon, hence:

$$D \propto \frac{1}{\sqrt{\lambda}} \tag{11}$$

Thus, we can place an upper-bound on the width of our detector:

$$w < \frac{c_1}{\sqrt{\lambda}} \tag{12}$$

This constant, c_1, has been experimentally found to be $1.5 \times 10^{-10} m^{3/2}$ [14], which corresponds to a width of approximately 188 nm for our 637 nm photons.

A more refined approach for an upper-bound was suggested by J.J. Renema based on the work of Lusche [13], which makes use of the hotspot model. In Figure 4, we see the cut-off wavelength as a function of width based on various models. The hotspot model, indicated by the solid line, predicts that a cut-off wavelength of 637 nm corresponds to 130 nm wire width. We shall use this as our upper-bound.

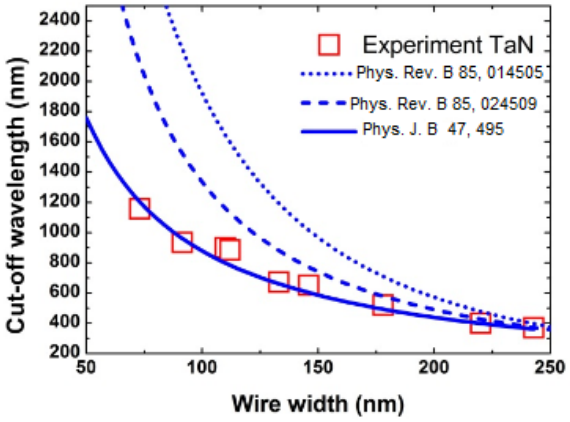

Figure 4: Cut-off wavelength as a function of width [13]. The solid blue line corresponds to the hotspot model.

Alexei Semenov also suggested in an email that we should not go beyond 120 nm based on the wavelength cut-off associated with the hotspot model.

The corners of the U-shape must also be rounded to avoid current crowding and reduction of the critical current [8]. The optimal geometry for the inner bend to help alleviate the reduction of critical current has a fill factor of 1/3, which follows the contour line of the separation between the current-crowding and current-expanding regions in a 180 degree turn, as seen in Figure 5 [3], which is given by the equation:

$$y = \pm \frac{2w}{\pi} cos^{-1}[exp\left(\frac{x\pi}{2w}\right)] \tag{13}$$

Where w is the width of the detector. However, this low fill factor reduces the absorption rate of the detector.

The purpose of a higher critical current is that the detection efficiency asymptotically approaches its ideal

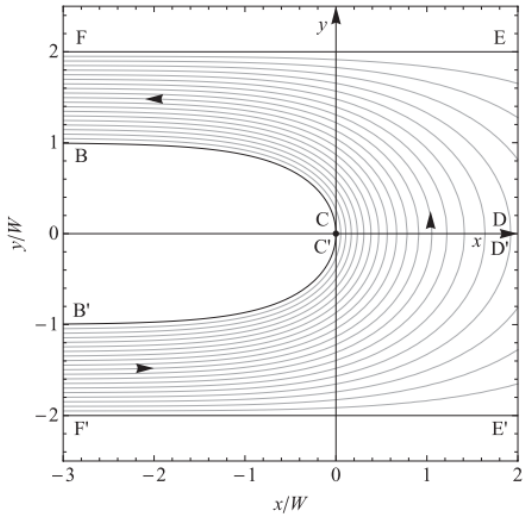

Figure 5: Optimal inner-bend curvature [3]. Axes are scaled to units of width.

quantity as a function of the bias current, and as one approaches the critical/depairing current, the rate of dark counts increases, hence being somewhere within the plateau region before the dark counts begin is ideal. As a trade-off between maximizing critical current and absorption rate, we set the fill-factor at 0.5.

J.J. Renema also suggests utilizing the field distribution of the photon based on a recently published paper [19]. In his paper, he argues that photons absorbed near the edges of the detector have a higher probability of registering a count, based on the notion that absorptions near the edge allow a higher probability of the entrance of vortices. His results show that these enhanced edge effects are seen up to 30 nm from the edge of the detector, suggesting an optimal width of 60 nm.

DEVICE EFFICIENCY AS A FUNCTION OF THE BIAS CURRENT, AND THE ISSUE OF DARK COUNTS

There are currently two papers in the literature that make use of superconducting nanowires in a diamond system [1, 17]. Atikian et. al. use NbTiN nanowires directly on diamond with both 1310 and 632 nm photons, while Rath et. al. use NbN nanowires on diamond rib-waveguide with 1550 nm photons. Rath et. al. reported an on chip device efficiency of 66% using a double meander design with a width of 100 nm and a length of 65 microns. Atikian et. al. do not report their efficiency.

Pernice et. al. [16] report the device efficiency as a function of the width and length for a NbN on Si system with 1550 nm wavelength photons, as seen in Figure 6.

We can see that the narrowest detector shows a more pronounced knee-like behavior, and the device efficiencies

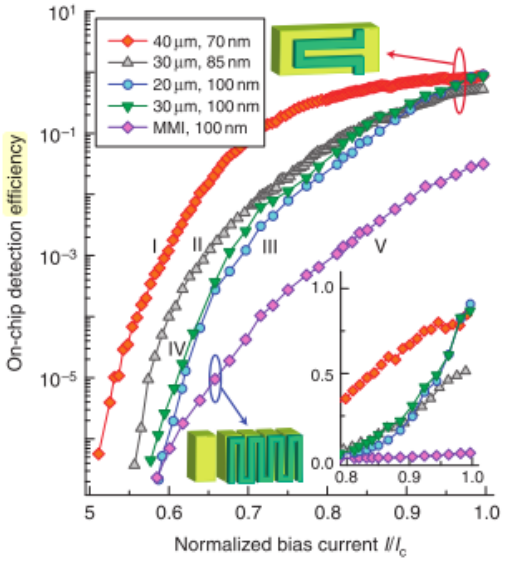

Figure 6: Device efficiencies as a function of width and length for 1550 nm photons [16]

of the other detectors only surpass it near the last few data points, where the 100 nm width shows the highest efficiency. Kahl et. al. report similar behavior with NbN on Si_3N_4 using telecom wavelengths [10] with an optimal width of 80 nm. For 768 nm light, Schuck et. al. report the highest efficiency for 75 nm width for a NbTiN on Si_3N_4 system, as we can see in Figure 7, though the 60 nm width wire has comparable device efficiency and lower noise equivalent power (NEP).

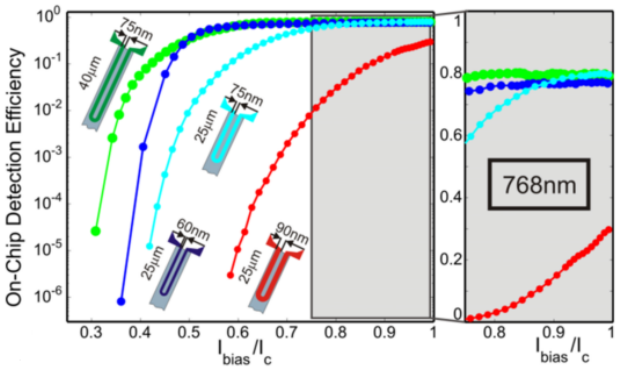

Figure 7: Device efficiency as a function of width and length for 768 nm photons [20].

Though the nature of dark counts is still debated [11], they begin to appear when the detector is biased near the critical current. Because the sharper knee bend is a feature of the narrower wires, it is important to consider this fact along with the device efficiency.

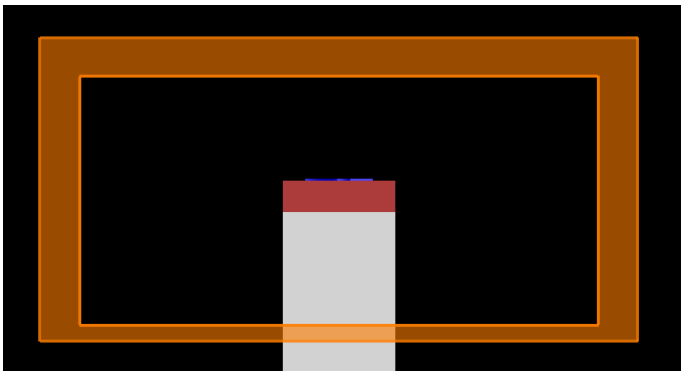

Figure 8: Simulation boundaries. The diamond layer meets the simulation boundary at 500 nm, the GaP is 140 nm thick, and the NbN detector is 5 nm thick. The width of the GaP and diamond layers are 500 nm.

METHODS

The Lumerical FDTD Solutions code was used for the simulations. We shall consider the x-coordinate the width, the y-coordinate the thickness, and the z-coordinate the length. The waveguide's propagation axis is along the z-direction. A base model of a 500 nm wide and 140 nm thick gallium phosphide layer is laid on top of a 500 nm wide diamond substrate, which is 500 nm in the -y direction to the simulation boundary (using perfectly matched layer boundary conditions, or PML), as seen in Figure 8. The diamond layer extends fully through the simulation boundary in the -y direction. The GaP and diamond extend fully through the PML in both z-directions. The detector begins 400 nm from the source, where the bend in the U is the nearest feature to the source.

The detector fully extends through the PML in the +z-direction. The distance between the start of the detector to the simulation boundary is 10 microns. The thickness of the wire is set at a constant 5 nm, while the width, fill-factor, and waveguide geometry is varied. The bend structure is 150 nm in length. The center-to-center difference between parallel sections of the detector is called the pitch. The ratio of the width of the detector over the pitch is called the fill-factor.

The source is the fundamental TE mode of the waveguide. The wavelength of the source was centered at 637 nm with a 15 nm span. The mode is injected along the z-axis in the center of the GaP layer. Power monitors were placed at the start of the detector, at the end of the bend structure, and at 1.25 micron intervals of the detector. A power monitor was also placed as a x-z plane slice through the GaP layer. The simulation boundaries were kept at least half a wavelength away from any structure features, except for the special instances listed above. The accuracy of the mesh was set to 4, and a 2 nm (x)

x 2 nm (y) override mesh was placed over the detector structure.

"Hard" n values were used for the GaP and diamond, 3.31 and 2.42, respectively. Ellipsometry data was used for the NbN refractive index [9].

RESULTS

Because the parameter space was too large (waveguide thickness, waveguide width, nanowire width, nanowire gap) in comparison to the simulation time, a multi-parameter sweep could not be done, and three parameters were fixed while the fourth was varied. In Figure 9, we see the electric field distribution at 5 microns into the detector.

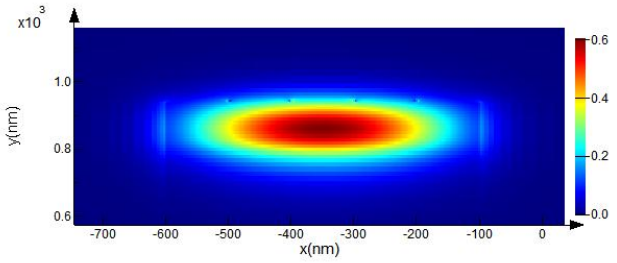

Figure 9: E field distribution at 5 microns into the detector.

We first examine the base model of 100 nm width, 5 nm thickness, 0.50 fill-factor, with a GaP waveguide of 140 nm by 500 nm. We vary the width of the detector while keeping the other parameters of the geometry constant. We find that the maximum absorption is attained for a width of 110 nm in Figure 10. We note that in the methods of Kovalyuk et. al. [12], they find a monotonically increasing absorption as a function of width. Their methods make use of a constant nanowire gap, which leads to an extremely sharp bend at higher nanowire widths at the U-turn. In lieu of this, our work will use a constant .5 fill-factor was chosen as a trade-off between absorption and maximum critical current. We also note that Schuck et. al. [20] reports that nearly all optical light was absorbed by 25 microns. We shall use this length as a benchmark figure. We find that even for the lowest absorption at 60 nm width, the absorption probability will be 98.00% for 25 microns. For the highest absorption rate at 110 nm width, the absorption probability will be 99.28% for 25 microns.

This maximum in the absorption rate was attributed to the gap between the nanowires separating sufficiently enough at the higher widths such that it begins to outweigh the increased width of the detector.

Next, we return to our base model and adjust the fill-factor. In Figure 11, we see the power absorbed as a

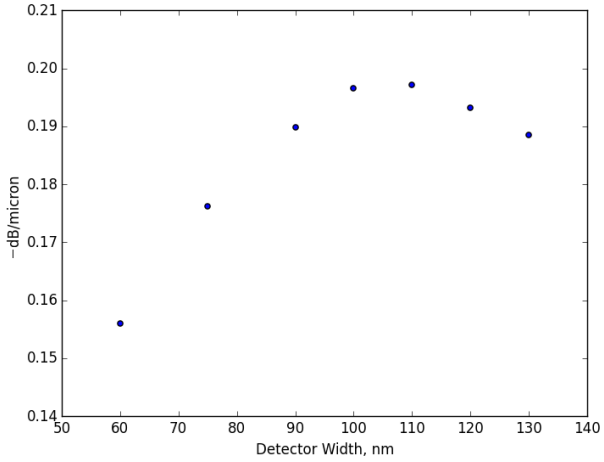

Figure 10: Power absorbed vs. the detector width

function of the distance between nanowires.

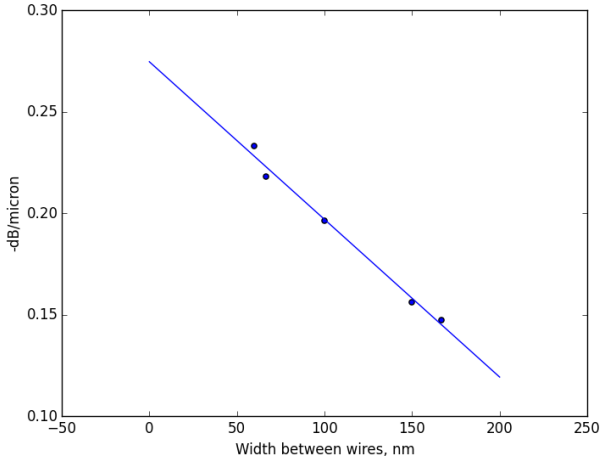

Figure 11: Power absorbed vs. the gap between nanowires (pitch-width)

Though there are not enough data points to tell conclusively, in Figure 11 we can potentially see that the absorption oscillates around the best fit line, with a wavelength on the order of 100 nanometers. We also see this effect with the GaP thickness in Figure 12, with roughly the same wavelength. In Figure 13, we see that the power absorbed peaks at 450 nm width waveguides.

The device detection efficiency is a complex interplay of competing values. A larger detector increases absorption, a lower fill-factor improves I_c but reduces absorption, and a smaller detector improves the registration probability and the efficiency plateau but lowers absorption. For the first round of detectors, a safe starting geometry would be 5 nm nanowire thickness, 100 nm nanowire width, 50% fill-factor, 500 nm waveguide width, and 40 microns

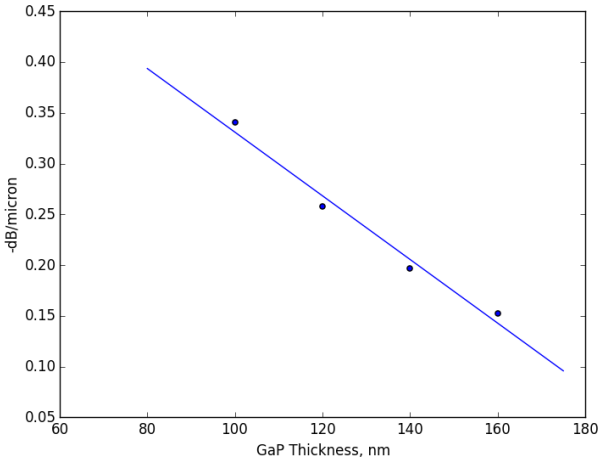

Figure 12: Power absorbed vs. the thickness of the Gallium Phosphide layer

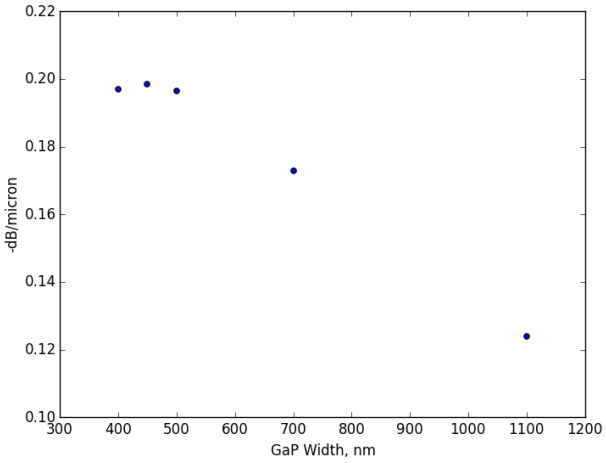

Figure 13: Power absorbed vs. gallium phosphide width

in length. A more calculated geometry taking advantage of the knee-like behavior would use 5 nm nanowire thickness, 60-80 nm nanowire width, 50% fill-factor, 450 nm waveguide width, and 25-30 microns in length.

CONCLUSION

We find that the use of waveguide-coupled niobium nitride superconducting single photon detectors shows promising absorption rates for 637 nm photons. Device fabrication will begin this fall, and with the higher energy optical photons, high device efficiencies are expected.

* University of Washington, REU
† joyshin@ucsc.edu

[1] Haig a. Atikian, Amin Eftekharian, a. Jafari Salim, Michael J. Burek, Jennifer T. Choy, a. Hamed Majedi, and Marko Lončar. Superconducting nanowire single photon detector on diamond. *Applied Physics Letters*, 104(12):1–5, 2014.

[2] Lilian Childress and Ronald Hanson. Diamond NV centers for quantum computing and quantum networks. *MRS Bulletin*, 38(02):134–138, 2013.

[3] John R. Clem and Karl K. Berggren. Geometry-dependent critical currents in superconducting nanocircuits. *Physical Review B - Condensed Matter and Materials Physics*, 84(17):1–27, 2011.

[4] Marcus W. Doherty, Neil B. Manson, Paul Delaney, Fedor Jelezko, Jörg Wrachtrup, and Lloyd C L Hollenberg. The nitrogen-vacancy colour centre in diamond. *Physics Reports*, 528(1):1–45, 2013.

[5] Andreas Engel, Julia Lonsky, Xiaofu Zhang, and Andreas Schilling. Detection Mechanism in SNSPD: Numerical Results of a Conceptually Simple, Yet Powerful Detection Model. *arXiv preprint arXiv:1408.4907*, 25(200021), 2014.

[6] Andreas Engel and Andreas Schilling. Numerical analysis of detection-mechanism models of superconducting nanowire single-photon detector. *Journal of Applied Physics*, 114(21), 2013.

[7] Andreas Engel, Alexei Semenov, Heinz Wilhelm Hübers, Kostya Il'In, and Michael Siegel. Fluctuations and dark count rates in superconducting NbN single-photon detectors. *Physica Status Solidi C: Conferences*, 2(5):1668–1673, 2005.

[8] H. L. Hortensius, E. F C Driessen, T. M. Klapwijk, K. K. Berggren, and J. R. Clem. Critical-current reduction in thin superconducting wires due to current crowding. *Applied Physics Letters*, 100(18), 2012.

[9] Xiaolong Hu. Efficient Superconducting-Nanowire Single-Photon Detectors and Their Applications in Quantum Optics. 2011.

[10] Oliver Kahl, Simone Ferrari, Vadim Kovalyuk, Gregory N. Goltsman, Alexander Korneev, and Wolfram H. P. Pernice. Waveguide integrated superconducting single-photon detectors with high internal quantum efficiency at telecom wavelengths. *Scientific Reports*, 5(February):10941, 2015.

[11] J. Kitaygorsky, I. Komissarov, a. Jukna, D. Pan, O. Minaeva, N. Kaurova, a. Divochiy, a. Korneev, M. Tarkhov, B. Voronov, I. Milostnaya, G. Gol'tsman, and Roman R. Sobolewski. Dark counts in nanostructured NbN superconducting single-photon detectors and bridges. *IEEE Transactions on Applied Superconductivity*, 17(2):275–278, 2007.

[12] V Kovalyuk, W Hartmann, O Kahl, N Kaurova, a Korneev, G Goltsman, and W H P Pernice. Absorption engineering of NbN nanowires deposited on silicon nitride nanophotonic circuits. *Optics express*, 21(19):22683–92, 2013.

[13] R. Lusche, a. Semenov, K. Ilin, M. Siegel, Y. Korneeva, a. Trifonov, a. Korneev, G. Goltsman, D. Vodolazov, and H. W. Hübers. Effect of the wire width on the intrinsic detection efficiency of superconducting-nanowire single-

photon detectors. *Journal of Applied Physics*, 116(4):1–16, 2014.

[14] L. Maingault, M. Tarkhov, I. Florya, a. Semenov, R. Espiau De Lamaëstre, P. Cavalier, G. Gol'Tsman, J. P. Poizat, and J. C. Vilgier. Spectral dependency of superconducting single photon detectors. *Journal of Applied Physics*, 107(11):2008–2011, 2010.

[15] C.M. Natarajan, M.G. Tanner, and R. Hadfield. Superconducting nanowire single-photon detectors: physics and applications. 063001, 2012.

[16] W H P Pernice, C Schuck, O Minaeva, M Li, G N Goltsman, a V Sergienko, and H X Tang. High-speed and high-efficiency travelling wave single-photon detectors embedded in nanophotonic circuits. *Nature communications*, 3:1325, 2012.

[17] Patrik Rath, Oliver Kahl, Simone Ferrari, Fabian Sproll, Georgia Lewes-malandrakis, Dietmar Brink, Konstantin Ilin, Michael Siegel, Christoph Nebel, and Wolfram Pernice. Superconducting single photon detectors integrated with diamond nanophotonic circuits.

[18] J. J. Renema, R. Gaudio, Q. Wang, Z. Zhou, a. Gaggero, F. Mattioli, R. Leoni, D. Sahin, M. J a De Dood, a. Fiore, and M. P. Van Exter. Experimental test of theories of the detection mechanism in a nanowire superconducting single photon detector. *Physical Review Letters*, 112(11):1–5, 2014.

[19] J. J. Renema, Q. Wang, R. Gaudio, I. Komen, K. op t Hoog, D. Sahin, a. Schilling, M. P. van Exter, a. Fiore, a. Engel, and M. J. a. de Dood. Position-Dependent Local Detection Efficiency in a Nanowire Superconducting Single-Photon Detector. *Nano Letters*, page 150626122808004, 2015.

[20] Carsten Schuck, Wolfram H P Pernice, and Hong X Tang. Waveguide integrated low noise NbTiN nanowire single-photon detectors with milli-Hz dark count rate. *Scientific reports*, 3:1893, 2013.

[21] a V Semenov, a a Korneev, and G N Goltsman. Vortex assisted mechanism of photon counting in superconducting nanowire single photon detector revealed by external magnetic field. pages 1–11, 2015.

[22] Alexei D. Semenov, Philipp Haas, Heinz Wilhelm Hübers, Konstantin Ilin, Michael Siegel, Alexander Kirste, Thomas Schurig, and Andreas Engel. Vortex-based single-photon response in nanostructured superconducting detectors. *Physica C: Superconductivity and its Applications*, 468(7-10):627–630, 2008.

[23] M Suzuki and Is Suzuki. Lecture Note on Solid State Physics Ginzburg-Landau Theory for Superconductivity. *. . . of Physics, State University of New York at . . .*, pages 1–105, 2007.

[24] Nicole Thomas, Russell J Barbour, Yuncheng Song, Minjoo Larry Lee, and Kai-Mei C Fu. Waveguide-integrated single-crystalline GaP resonators on diamond. *Optics express*, 22(11):13555–64, 2014.

[25] M Šindler, R Tesa, J Koláček, P Szabó, P Samuely, V Hašková, C Kadlec, F Kadlec, and P Kužel. Far-infrared electrodynamics of thin superconducting NbN film in magnetic fields. *Superconductor Science and Technology*, 27(5):055009, 2014.

[26] A N Zotova and D Y Vodolazov. Photon detection by current-carrying superconducting film: A time-dependent Ginzburg-Landau approach. *Physical Review B - Condensed Matter and Materials Physics*, 85(2):1–9, 2012.